JOURNAL OF APPLIED PHYSICS **114**, 214901 (2013)

Electric-field-coupled resonators as metamaterial loadings for waveguide miniaturization

H. Odabasi[a] and F. L. Teixeira[b]
ElectroScience Laboratory and Department of Electrical and Computer Engineering, The Ohio State University, Columbus, Ohio 43202, USA

(Received 23 August 2013; accepted 13 November 2013; published online 2 December 2013)

We show that a rectangular metallic waveguide loaded with metamaterial elements consisting of electric-field-coupled (ELC) resonators placed at the sidewalls can operate well below the cutoff frequency of the respective unloaded waveguide. For the example considered of a waveguide with square cross-section and original TE-mode cut-off frequency at 16.67 GHz (under no loading), a TE-mode passband is obtained around 8.6 GHz once the waveguide is loaded with ELC resonators. Similarly, for TM-mode excitation with original cut-off at 23.57 GHZ, TM-mode passbands are obtained around 8.5 GHz and 11.3 GHz, for two different orientations of ELC resonators. The dispersion diagrams indicate that propagating modes in ELC-loaded waveguides are of forward-type for both TE and TM modes. We also study the dispersion diagram and transmission characteristics of rectangular metallic waveguides simultaneously loaded with both ELCs and split ring resonators. Such "doubly"-loaded waveguides can support both forward wave and backward waves and provide independent control of the propagation characteristics for the respective modes.
 [http://dx.doi.org/10.1063/1.4837597]

I. INTRODUCTION

The study of metallic waveguides loaded with metamaterials has attracted much interest.[1–31] Because a rectangular waveguide behaves as an electric plasma for TE modes below cutoff,[1] such waveguide can exhibit left-handed media behavior when loaded with negative permeability materials.[1–4] In particular, waveguides loaded with split-ring resonators (SRRs) providing negative permeability were studied extensively.[1,2,10–20,22] One important feature of negative permeability material-loaded waveguides is that they support propagation of backward waves. However, it is noteworthy that the anisotropic characteristics of the metamaterial loadings plays a crucial role in the wave behavior and transmission.[3,4,6,9,10,22] In fact, this is precisely the reason why a waveguide with an isotropic negative permeability material loading does not support guided modes.[6] Thus, in order to produce backward wave propagation, the transverse magnetic permeability needs to be negative, whereas a negative longitudinal permeability produces forward waves. This change in transmission response was recently exploited for controlling backward and forward waves in SRR-loaded waveguides by means of a rotation on the SRR elements.[22] Loadings such as ferrites and dielectric-filled corrugations were also proposed for realization of left-handed media.[26–29] Besides yielding left-handed behavior, metamaterial loadings also enable waveguide miniaturization.[6,10,12,13,21,22] Though most of the research has focused on SRR-loaded waveguides, other types of metamaterial loadings are also effective.[6–9,12,15,18,23,26–29]

It is also of interest to study what occurs when a metallic waveguide is loaded with negative permittivity media. It can be easily shown that negative permittivity does not produce a passband for TE modes while very high values of permittivity lead to a passband. On the other hand, by invoking the duality between TE and TM modes, it can be shown that rectangular waveguides behave as magnetic plasma for TM modes below cutoff.[7–9] Hence, when loaded with negative permittivity media, they mimic left-handed media. In particular, wire media providing negative permittivity was proposed to enable backward waves for TM modes.[7,8] Experimental results on backward waves for TM modes were presented in Ref. 9.

Different methods (under various levels of approximation) have been used to understand transmission phenomena in waveguides with metamaterial loadings that occurs below (empty-waveguide) cutoff frequency.[9,10,17,22] Many of the described prior work rely on an effective medium approximation, where the effect of discrete metamaterial elements is approximated by a homogeneous anisotropic medium. Though an effective medium approximation does not explain the phenomena completely, it can give an useful qualitative description of the physics. In another approach,[6,15] it was shown that the transmission properties in resonant-scatterer-loaded waveguides are governed by the properties of periodical array of resonant dipoles. In particular, the dispersion properties of waveguides loaded with electric and magnetic scatterers were studied for different orientations.[6,15]

As discussed above, electric scatterers (resonators) can also provide passband(s) below the cut-off. Here, we investigate miniaturization of waveguides loaded with electric-field-coupled (ELC) resonators, for both TE and TM modes. ELC resonators were proposed[32] to yield negative permittivity and can be used as an attractive alternative to early

[a]Current address: Center for Metamaterials and Integrated Plasmonics, Duke University, Durham, North Carolina 27706, USA
[b]Author to whom correspondence should be addressed. Email: teixeira.5@osu.edu

proposed wire media and inductively loaded short wires or strips.[6,7,15] ELC has the advantage of easily tunable response and excitation under different polarizations, enabling different resonant frequencies and characteristics. This feature of ELC was recently exploited for the design electrically small antennas,[33] in conjunction with complementary-electric-field-coupled (CELC) resonators.[34] Most of the prior work on metamaterial-loaded waveguides has considered a "homogeneous" type of loading, i.e., where one single element type is used. We show that waveguides simultaneously loaded with ELC and SSR resonators can support both backward and forward modes below the original cutoff frequency. In this case, each resonator type can provide independent control of the respective propagating modes.

II. RESULTS AND DISCUSSION

Fig. 1(a) shows a {ELC+SRR}-loaded metallic waveguide, employing a coaxial excitation of TE modes. It was shown elsewhere that the transmission can be significantly enhanced when a properly designed coaxial-cable excitation is used.[16] The waveguide has 9×9 mm cross section and 74 mm length along the propagation direction. The cut-off frequency of the respective empty waveguide is 16.66 GHz for the TE_{10} mode and 23.57 GHz for the TM_{11} mode. As indicated in Fig. 1(a), the ELC resonators are placed at the lateral sides of the waveguide and the SRR resonators are placed along the center axis of the waveguide. We use a broadside-coupled SRR (BC-SRR) configuration.[22,35] The ELC resonators are placed such that they are excited by the vertical component of the electric field of the dominant mode. Likewise, the SRR resonators are placed such that they are excited by the transverse component of the magnetic field of the dominant mode. Figs. 1(b) and 1(c) show schematics of ELC and SRR elements, respectively. Referring to Figs. 1(b) and 1(c), the dimensions of the ELC resonator are as follows: $l = 6$ mm, $w = 0.8$ mm, $g = 0.8$ mm, and $t = 2.4$ mm. Similarly, for the SRR resonator, we have $r = 4$ mm, $s = 1$ mm, and $d = 0.8$ mm. The resonators are backed by a dielectric substrate with $\epsilon_r = 2.2$ and loss tangent $\tan\delta = 0.001$. The thickness of the substrate is 0.5 mm. The inner wire of the coaxial feed has 0.5 mm radius and it extends 8 mm inside the waveguide. The coaxial cable has 1.7 mm outer radius and dielectric constant of 2.1. All simulations are performed using the time-domain solver of CST Microwave Studio™ (MWS) modeling software, based on the finite integration technique. The dispersion diagrams are calculated through the eigensolver of MWS, with periodic boundary condition (except for a phase shift) assigned long the z direction.

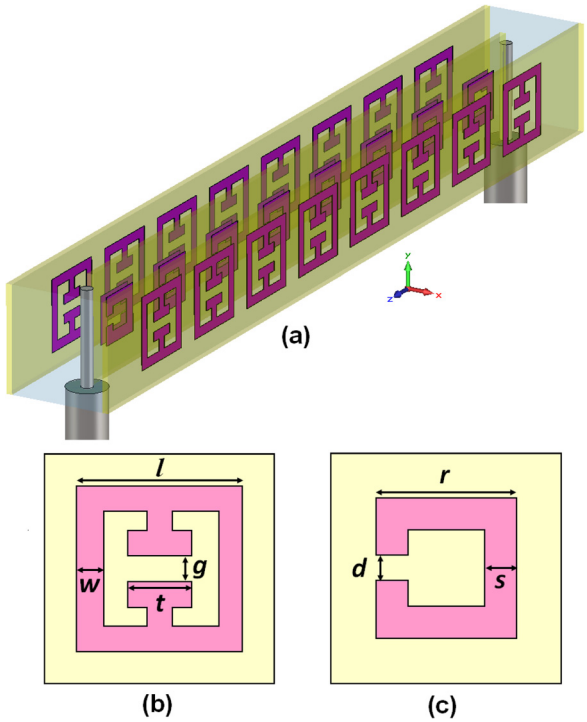

FIG. 1. Configuration of a {ELC+SRR}-loaded rectangular waveguide. The ELC resonators are placed at the lateral walls, while the SRR resonators are placed along the center of the waveguide. Schematics of (b) ELC resonator and (c) SRR resonator.

Fig. 2 shows TE-mode dispersion diagrams for ELC-, SRR-, and {ELC+SRR}-loaded waveguides, respectively. The insets depict the unit cell configurations of the ELC and SRR cases, respectively. In the {ELC+SRR} case, the ELC and SRR resonators are simply placed as shown and combined into one unit cell. The unit cell dimensions are 9×9 mm in the x and y (transverse) directions and 8 mm in the z (longitudinal) direction. We first consider the lossless case where the dielectric substrate is assumed lossless and the metallic components are modeled as perfect electrical conductor (PEC). For the SRR-loaded waveguide, we observe the well-known negative-slope characteristic of a backward wave; whereas for the ELC-loaded waveguide, we observe a positive-slope characteristic of a forward wave. When the waveguide is loaded with both SRR and ELC resonators, the first passband around 6.7 GHz virtually overlaps with that of the SRR-loaded waveguide while the second passband around 8.6 GHz virtually overlaps with that of the ELC-loaded waveguide, showing that the passband of the backward waves and forward waves can be controlled

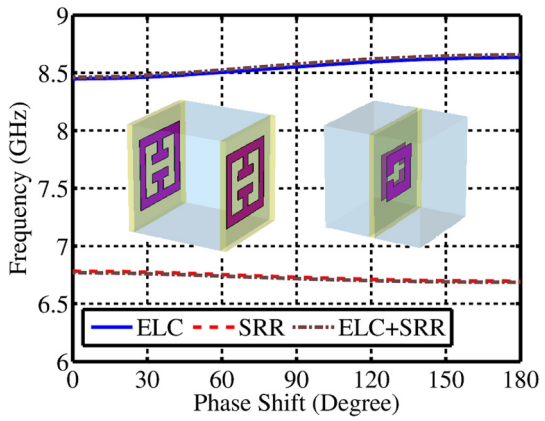

FIG. 2. TE-mode dispersion diagrams of ELC-, SRR-, and {ELC+SRR}-loaded waveguides. As seen, the SRR-loaded waveguide supports backward waves below cutoff whereas the ELC-loaded waveguide supports forward waves. The first and second passbands of the {ELC+SRR}-loaded waveguide nearly match the passbands of the SRR-loaded and ELC-loaded waveguides, respectively. The insets show the unit cell configuration of the ELC and SRR resonator cases.

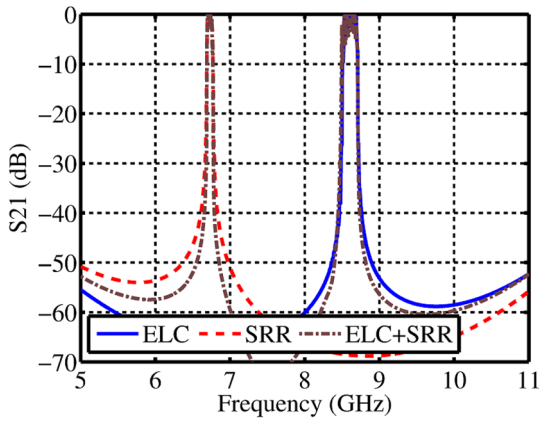

FIG. 3. TE-mode transmission spectra for ELC-, SRR-, and {ELC+SRR}-loaded waveguides for lossless case. For the {ELC+SRR}-loaded waveguide, the two transmission peaks observed nearly match the peaks of the SRR-loaded and ELC-loaded waveguides, respectively.

independently. Fig. 3 shows the corresponding transmission spectrum for lossless case, which matches very well passband frequencies around 6.7 GHz and 8.6 GHz in the dispersion diagrams shown in Fig. 2. In all three cases, we observe total transmission (more visible in Fig. 4). The -3 dB fractional bandwidth for the SRR loaded waveguide is about 1% and for the ELC loaded waveguide is about 2%.

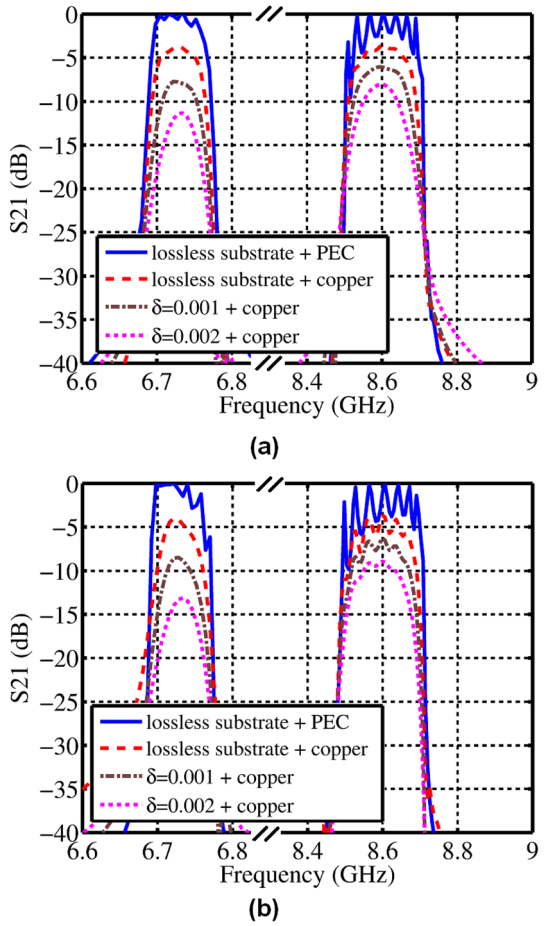

FIG. 4. Effect of losses on the TE-mode transmission spectra for (a) ELC- and SRR-loaded waveguides (rightmost and leftmost passbands, respectively) and for (b) {ELC+SRR}-loaded waveguide. Conductive loss on the metals and dielectric losses are added sequentially.

We next study the effect of losses in the system. Fig. 4(a) shows a zoomed-in view of the transmission spectrum around the two passbands. As expected, only in the case of zero losses total transmission can be obtained. Conduction losses are added into the system by modeling metallic parts as Cu, with conductivity $\sigma = 5.8 \times 10^7$ S/m. Dielectric losses are subsequently added, as indicated in Fig. 4, by considering two types of substrates: the first one being a dielectric material with loss tangent $\tan\delta \approx \delta = 0.001$, and the second one being a dielectric material with $\tan\delta \approx \delta = 0.002$. Note that for both ELC and SRR loaded waveguide, the effect of conductive losses are quite similar; however, for dielectric losses, the effect is more pronounced for the SRR-loaded waveguide. Fig. 4(b) shows the same analysis for {SRR+ELC}-loaded waveguide (where the two passbands appear simultaneously).

Fig. 5 shows the normalized electric-field distribution along the lateral walls of the ELC-loaded waveguide, with a zoomed-in view of an individual ELC element. Note that the field is strongly concentrated between the gap of the two center ELC arms. This corresponds to the fundamental characteristic mode of the ELC resonator,[32] excited by the electric field component perpendicular to the gap. An ELC resonator can also be excited by an electric field component parallel to the gap. This will be discussed in the following example. Since SRR-loaded waveguides were extensively studied in the literature, we do not discuss the excitation mechanism in any detail here.

Fig. 6 shows another ELC-loaded waveguide configuration, now with coaxial excitation of TM modes. The waveguide has 9×9 mm cross-section and 64 mm length. In this case, we insert ELC resonators at the four walls in view of the TM_{11} mode distribution. Moreover, we simulate two

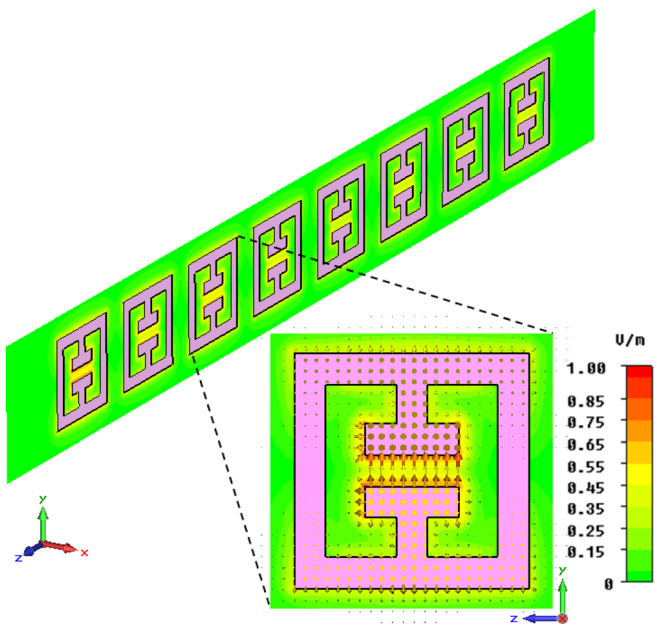

FIG. 5. Normalized electric field distribution along the sidewall of the waveguide with ELC resonators under TE mode excitation, with a zoomed-in view around an individual resonator. In this TE case, it is observed that the field is largely confined in the gaps between the two central segments of the ELC resonator.

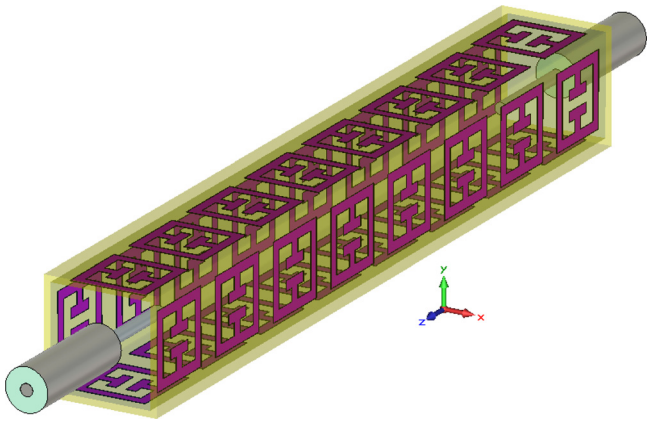

FIG. 6. Rectangular waveguide loaded with ELC resonators placed on all four sidewalls, under TM mode excitation. Two orientations are considered for the ELC resonators. The first orientation is the one shown in the figure (ELC-1). The second orientation has the lateral-walls ELC resonators rotated by 90° along the x direction and the top/bottom-walls ELC resonators rotated by 90° along the y direction (ELC-2).

different ELC orientations: The first orientation (ELC-1) is identical to before, whereas the second orientation (ELC-2) has the ELC resonators rotated by a 90° angle (while remaining parallel to the walls). Fig. 7 shows the TM-mode dispersion diagrams for these two waveguide configurations, with the passband for ELC-1 at around 11.3 GHz and the passband for ELC-2 around 8.5 GHz. Both passbands correspond to forward waves. Fig. 7 also shows the dispersion diagram in the case where ELC-resonators are placed *only* at the two lateral sidewalls of the waveguide. It is seen that the laterally loaded case also supports wave propagation under TM mode excitation; however, the bandwidth (and transmission) degrade slightly in this case. Fig. 8 shows the corresponding transmission spectra for both orientations. For ELC-2, the transmission peak is noticeably weaker. Since ELC resonators cannot be excited via an electric field component perpendicular to the ELC-resonator plane, both ELC orientations considered here are excited by an electric field component along the propagation direction. Thus, the ELC-2 passband in the TM case and the ELC passband in the TE case correspond to the excitation of same characteristic mode of the ELC resonator.

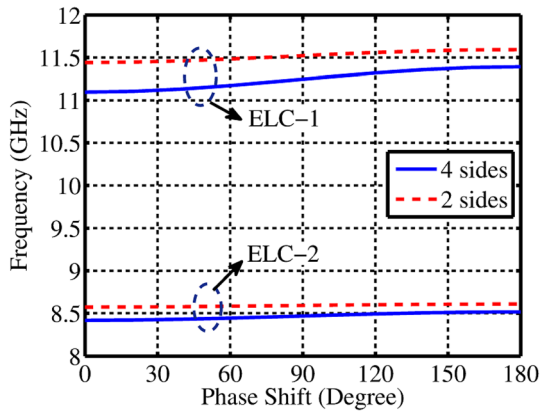

FIG. 7. TM-mode dispersion diagrams of ELC-1 and ELC-2 loaded waveguides. As seen, both orientations support forward waves.

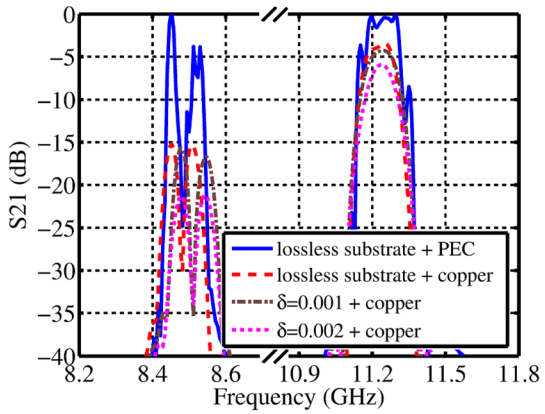

FIG. 8. TM-mode transmission spectra for ELC-1 (higher passband) and ELC-2 (lower passband) loaded waveguides. The performance of the ELC-1 configuration is considerably less impacted by material losses.

Fig. 9 shows the normalized electric field distribution along the lateral and bottom walls containing the ELC resonators. The inset shows a zoomed-in view of an individual ELC resonator at the lateral wall. Note that in this case, the field is more confined in the gap between adjacent ELC resonators. The field distribution around each side resonators is nearly identical. The field distribution for the ELC-2 case is very similar to the TE mode case and hence is not shown here.

Similarly to most types of waveguide loadings, the use of metamaterial resonators can have an adverse effect on power handling capabilities. Miniaturization *per se* also has an adverse impact on power handling. For high-power applications, this adverse effect can be typically compensated by independent means such as pressurization and/or cooling. A detailed discussion of specific applications of the proposed ELC-loaded waveguide configurations is beyond the scope of this paper, but it can be noted that the transmission

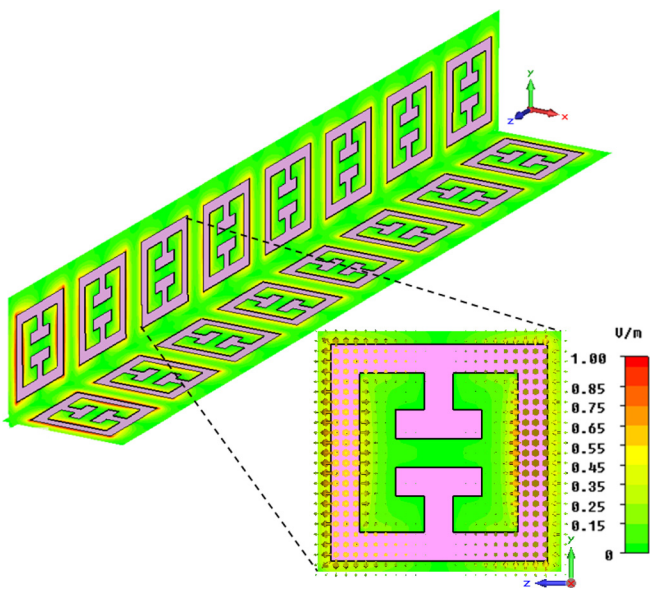

FIG. 9. Normalized electric field distribution along the sidewall of the waveguide with ELC resonators under TM mode excitation, with a zoomed-in view around an individual resonator. In this TM-case, it is observed that in the field is largely confined in the gaps between adjacent ELC resonators.

characteristics of such waveguides makes them suited to use not simply as guiding structures but as bifunctional front-end elements that could support, for example, tunable passband-filter capabilities.

III. CONCLUDING REMARKS

It was shown that ELC-loaded waveguides can support forward waves below the (original, empty-waveguide) cutoff frequency under TE or TM excitation. For the example considered in this paper, of a waveguide with square cross-section and original TE-mode cut-off frequency equal to 16.67 GHz under no loading, a TE-mode passband is obtained around 8.6 GHz once the waveguide is loaded with ELC resonators. Similarly, for TM mode excitation where the original cut-off frequency is equal to 23.57 GHZ, TM-mode passbands are obtained around 8.5 GHz and 11.3 GHz, for two different orientations of the ELC resonators. Since, for a square waveguide, the cross-section area is inversely proportional to the square of the cut-off frequency, the equivalent miniaturization factors obtained here are equal to approximately 3.8 in the TE example, and approximately 7.7 and 4.4 in the TM examples. Moreover, when loading metallic waveguides with both ELC and SRR resonators, both forward and backward propagating modes can be simultaneously produced below cutoff, and each mode can be independently controlled by changing the dimensions of the respective (ELC or SRR) resonators. Based on the results presented, we conclude that loading metallic waveguides with ELC resonators can provide an effective miniaturization strategy.

[1]R. Marqués, J. Martel, F. Mesa, and F. Medina, Phys. Rev. Lett. **89**, 183901 (2002).
[2]R. Marqués, J. Martel, F. Mesa, and F. Medina, Microwave Opt. Technol. Lett. **35**, 405 (2002).
[3]I. G. Kondrat'ev and A. I. Smirnov, Phys. Rev. Lett. **91**, 249401 (2003).
[4]R. Marqués, J. Martel, F. Mesa, and F. Medina, Phys. Rev. Lett. **91**, 249402 (2003).
[5]F. Falcone, F. Martin, J. Bonache, R. Marques, and M. Sorolla, Microwave Opt. Technol. Lett. **40**, 3 (2004).
[6]P. A. Belov and C. R. Simovski, Phys. Rev. E **72**, 036618 (2005).
[7]J. Esteban, C. Camacho-Penalosa, J. Page, T. Martin-Guerrero, and E. Marquez-Segura, IEEE Trans. Microwave Theory Tech. **53**, 1506 (2005).
[8]I. S. Nefedov, X. Dardenne, C. Craeye, and S. A. Tretyakov, Microwave Opt. Technol. Lett. **48**, 2560 (2006).
[9]H. Xu, Z. Wang, J. Hao, J. Dai, L. Ran, J. A. Kong, and L. Zhou, Appl. Phys. Lett. **92**, 041122 (2008).
[10]S. Hrabar, J. Bartolic, and Z. Sipus, IEEE Trans. Antennas Propag. **53**, 110 (2005).
[11]J. D. Baena, L. Jelinek, R. Marqués, and F. Medina, Phys. Rev. B **72**, 075116 (2005).
[12]G. Lubkowski, C. Damm, B. Bandlow, R. Schuhmann, M. Schussler, and T. Weiland, in *36th European Microwave Conference, 2006* (2006), pp. 1312–1315.
[13]S. Hrabar and G. Jankovic, Microwave Opt. Technol. Lett. **48**, 2587 (2006).
[14]Q. Wu, F.-Y. Meng, J. Wu, and L.-W. Li, Appl. Phys. A **87**, 305 (2007).
[15]G. Lubkowski, C. Damm, B. Bandlow, R. Schuhmann, M. Schussler, and T. Weiland, IET Microwaves, Antennas Propag. **1**, 165 (2007).
[16]J. Carbonell, L. J. Rogla, V. E. Boria, and R. Marques, J. Appl. Phys. **102**, 044902 (2007).
[17]S. Antipov, L. Spentzouris, W. Liu, W. Gai, and J. G. Power, J. Appl. Phys. **102**, 034906 (2007).
[18]G. Lubkowski, C. Damm, B. Bandlow, R. Schuhmann, M. Schubler, and T. Weiland, in *38th European Microwave Conference, EuMC 2008* (2008), pp. 1050–1053.
[19]E. Rajo-Iglesias, O. Quevedo-Teruel, and M. Kehn, IEEE Trans. Antennas Propag. **57**, 1571 (2009).
[20]O. Quevedo-Teruel, E. Rajo-Iglesias, and M. Ng Mou Kehn, IET Microwaves, Antennas Propag. **3**, 1262 (2009).
[21]F. L. Teixeira, H. Odabasi, and K. F. Warnick, J. Opt. Soc. Am. B **27**, 1603 (2010).
[22]F.-Y. Meng, Q. Wu, D. Erni, and L.-W. Li, IEEE Trans. Antennas Propag. **59**, 3400 (2011).
[23]Y.-D. Dong, T. Yang, and T. Itoh, IEEE Trans. Microwave Theory Tech. **57**, 2211 (2009).
[24]H. Xu, Q. He, S. Xiao, B. Xi, J. Hao, and L. Zhou, J. Appl. Phys. **109**, 023103 (2011).
[25]F. Chen, X. Wang, A. Hosseinzadeh, and E. Semouchkina, in *2012 IEEE Antennas and Propagation Society International Symposium (APSURSI)* (2012), pp. 1–2.
[26]T. Ueda and M. Tsutsumi, IEEE Trans. Magn. **41**, 3532 (2005).
[27]I. Eshrah, A. Kishk, A. Yakovlev, and A. Glisson, IEEE Trans. Microwave Theory Tech. **53**, 3298 (2005).
[28]I. Eshrah, A. Kishk, A. Yakovlev, and A. Glisson, IEEE Trans. Antennas Propag. **53**, 3673 (2005).
[29]T. Ueda, A. Lai, and T. Itoh, IEEE Trans. Microwave Theory Tech. **55**, 1280 (2007).
[30]B. Edwards, A. Alù, M. E. Young, M. Silveirinha, and N. Engheta, Phys. Rev. Lett. **100**, 033903 (2008).
[31]B. Edwards, A. Alu, M. G. Silveirinha, and N. Engheta, J. Appl. Phys. **105**, 044905 (2009).
[32]D. Schurig, J. J. Mock, and D. R. Smith, Appl. Phys. Lett. **88**, 041109 (2006).
[33]H. Odabasi, F. L. Teixeira, and D. O. Guney, J. Appl. Phys. **113**, 084903 (2013).
[34]T. H. Hand, J. Gollub, S. Sajuyigbe, D. R. Smith, and S. A. Cummer, Appl. Phys. Lett. **93**, 212504 (2008).
[35]R. Marqués, F. Medina, and R. Rafii-El-Idrissi, Phys. Rev. B **65**, 144440 (2002).